

nuclei and subsequently added WGA to seal the existing pores. A nucleoplasmic signal was detectable when these nuclei were stained with α Nup133 and α Nup160 (24). In contrast to mock-depleted cytosol, Nup107-160-depleted cytosol did not induce the assembly of new pores (Fig. 3C). This lack of activity was caused by the absence of Nup107-160, because the addition of purified Nup107-160 complex (fig. S2C) restored NPC insertion (Fig. 3C).

Nuclei were formed in the presence of BAPTA (1,2-bis(2-aminophenoxy)ethane- N,N,N',N' -tetraacetic acid), a calcium chelator that inhibits NPC formation (25), and a strong nucleoplasmic Nup133 signal was detected (Fig. 3D). When the BAPTA nuclei were diluted in mock-depleted cytosol, NPC insertion was restored, whereas Nup107-160-depleted cytosol failed to do so (Fig. 3D). Consistent with the cytoplasmic RanGTP-mediated release of Importin β from the Nup107-160 complex, we found that the addition of 5 μ M RanT24N resulted in a 60% increase of Importin β associated with immunoprecipitated Nup107-160 complex (24). Thus, the incorporation of the Nup107-160 complex into new assembly sites occurs from both sides of the NE. Because nuclear transport is not required for NPC insertion in vitro, the nucleoplasmic pool of Nup107-160 complexes might be generated via chromatin association during nuclear assembly (17).

Next we wanted to analyze if pores assemble de novo or by the splitting of existing pores (7–9). We assembled NE-0 nuclei and subsequently fluorescently labeled individual pores with WGA-488 (green) (Fig. 4A). Upon dilution, WGA-488 remained stably bound to NPCs while new unlabeled pores were inserted (fig. S3A), which could be labeled with WGA-568 (red). Newly formed pores were only labeled with WGA-568 and appeared as red dots, whereas old pores were labeled with both dyes resulting in a yellow overlay. The new pores did not exhibit green signal from existing pores, suggesting that NPCs form de novo (Fig. 4A). When the formation of new pores was blocked by the addition of 5 μ M RanT24N, all pores appeared yellow in the overlay (Fig. 4A), indicating that red dots represented newly formed pores. Furthermore, the average fluorescence intensity of WGA-488-labeled NPCs remained constant after dilution of the dye, and it was indistinguishable between nuclei that inserted new pores and nuclei where the formation of new NPCs was blocked by 5 μ M RanT24N (fig. S3B). These results suggest that newly formed pores do not incorporate nucleoporins from existing NPCs, and they support a de novo mechanism, because in a splitting process, the intensity of the old pores would be expected to decrease. Additionally, we were able to detect pores that stained with α POM121, a transmembrane nucleoporin, and Nup133,

but not with mAb414 (fig. S3C). POM121 colocalized with mAb414 when the formation of new NPCs was blocked by RanT24N (fig. S3C). This indicates that phenyl-glycyl-repeat nucleoporins are recruited to new assembly sites after POM121 and Nup107-160 complexes have been incorporated and further supports de novo formation.

To determine whether NPC formation in vivo also occurs by a de novo mechanism, we generated a stable HeLa cell line expressing low, nontoxic levels of POM121 containing multiple copies of green fluorescent protein (GFP) to visualize individual NPCs in living cells (26). Four-dimensional confocal time-lapse microscopy was used to follow NPC assembly during interphase and new pores became visible as single dots in areas where initially no GFP signal was detectable (Fig. 4B and Movie S1) and in areas where preexisting pores have been photobleached (Fig. 4D). New NPCs colocalized with neighboring, preexisting pores along the z axis (fig. S4, A and B), showing that they were inserted into the NE. Consistent with de novo formation, existing pores did not change fluorescence intensity over time (Fig. 4C). These findings further support a de novo mechanism for NPC biogenesis.

References and Notes

1. S. R. Wentz, *Science* **288**, 1374 (2000).
2. D. Gorlich, U. Kutay, *Annu. Rev. Cell Dev. Biol.* **15**, 607 (1999).
3. G. G. Maul, L. L. Deaven, J. J. Freed, G. L. Campbell, W. Becak, *Cytogenet. Cell Genet.* **26**, 175 (1980).
4. G. G. Maul *et al.*, *J. Cell Biol.* **55**, 433 (1972).
5. M. Winey, D. Yarar, T. H. Giddings Jr., D. N. Mastrorade, *Mol. Biol. Cell* **8**, 2119 (1997).
6. B. Burke, J. Ellenberg, *Nat. Rev. Mol. Cell Biol.* **3**, 487 (2002).
7. M. Hetzer, T. C. Walther, I. W. Mattaj, *Annu. Rev. Cell Dev. Biol.* (2005).

8. K. Bodoor *et al.*, *Biochem. Cell Biol.* **77**, 321 (1999).
9. G. Rabut, P. Lenart, J. Ellenberg, *Curr. Opin. Cell Biol.* **16**, 314 (2004).
10. M. J. Lohka, Y. Masui, *Science* **220**, 719 (1983).
11. M. Hetzer, D. Bilbao-Cortes, T. C. Walther, O. J. Gruss, I. W. Mattaj, *Mol. Cell* **5**, 1013 (2000).
12. L. I. Davis, G. Blobel, *Proc. Natl. Acad. Sci. U.S.A.* **84**, 7552 (1987).
13. M. Dasso, *Curr. Biol.* **12**, R502 (2002).
14. C. Klebe, H. Prinz, A. Wittinghofer, R. S. Goody, *Biochemistry* **34**, 12543 (1995).
15. D. R. Finlay, E. Meier, P. Bradley, J. Horecka, D. J. Forbes, *J. Cell Biol.* **114**, 169 (1991).
16. A. Harel *et al.*, *Mol. Biol. Cell* **14**, 4387 (2003).
17. T. C. Walther *et al.*, *Nature* **424**, 689 (2003).
18. F. R. Bischoff, C. Klebe, J. Kretschmer, A. Wittinghofer, H. Ponstingl, *Proc. Natl. Acad. Sci. U.S.A.* **91**, 2587 (1994).
19. C. Klebe, F. R. Bischoff, H. Ponstingl, A. Wittinghofer, *Biochemistry* **34**, 639 (1995).
20. D. Gorlich, *Curr. Opin. Cell Biol.* **9**, 412 (1997).
21. K. J. Ryan, J. M. McCaffery, S. R. Wentz, *J. Cell Biol.* **160**, 1041 (2003).
22. A. Harel *et al.*, *Mol. Cell* **11**, 853 (2003).
23. T. C. Walther *et al.*, *Cell* **113**, 195 (2003).
24. M. A. D'Angelo, D. J. Anderson, E. Richard, M. W. Hetzer, data not shown.
25. C. Macaulay, D. J. Forbes, *J. Cell Biol.* **132**, 5 (1996).
26. N. Daigle *et al.*, *J. Cell Biol.* **154**, 71 (2001).
27. M. Hetzer *et al.*, *Nat. Cell Biol.* **3**, 1086 (2001).
28. Materials and methods are available as supporting material on Science Online.
29. G. Rabut, V. Doye, J. Ellenberg, *Nat. Cell Biol.* **6**, 1114 (2004).
30. Antibodies against Importin β were kindly provided by L. Gerace. We thank the members of our laboratory and T. Hunter for helpful discussions and W. Eckhart, J. Karlseder, V. Lundblad, J. Young, B. Sefton, and M. Weitzman for critically reading the manuscript. M.A.D. and M.H. were supported by The Pew Charitable Trust.

Supporting Online Material

www.sciencemag.org/cgi/content/full/312/5772/440/DC1
Materials and Methods
Figs. S1 to S4
Movie S1

22 December 2005; accepted 14 March 2006
10.1126/science.1124196

Differential Targeting of G $\beta\gamma$ -Subunit Signaling with Small Molecules

Tabetha M. Bonacci,¹ Jennifer L. Mathews,¹ Chujun Yuan,² David M. Lehmann,¹ Sundeep Malik,¹ Dianqing Wu,³ Jose L. Font,¹ Jean M. Bidlack,¹ Alan V. Smrcka^{1,2*}

G protein $\beta\gamma$ subunits have potential as a target for therapeutic treatment of a number of diseases. We performed virtual docking of a small-molecule library to a site on G $\beta\gamma$ subunits that mediates protein interactions. We hypothesized that differential targeting of this surface could allow for selective modulation of G $\beta\gamma$ subunit functions. Several compounds bound to G $\beta\gamma$ subunits with affinities from 0.1 to 60 μ M and selectively modulated functional G $\beta\gamma$ -protein-protein interactions in vitro, chemotactic peptide signaling pathways in HL-60 leukocytes, and opioid receptor-dependent analgesia in vivo. These data demonstrate an approach for modulation of G protein-coupled receptor signaling that may represent an important therapeutic strategy.

The $\beta\gamma$ subunits of heterotrimeric guanine nucleotide binding proteins (G proteins) are released upon ligand activation of G protein-coupled receptors (GPCRs). Free G $\beta\gamma$ subunits bind and regulate multiple target

proteins within the cell—including phospholipase C (PLC) β 2 and PLC β 3, phosphoinositide 3 kinase (PI3K) γ , adenylyl cyclase, N-type Ca²⁺ channels, and inwardly rectifying K⁺ channels—and mediate physiological

processes such as neutrophil chemotaxis, vascular cell proliferation, and cardiac chronotropy (1, 2).

To investigate the molecular nature of G $\beta\gamma$ -target recognition, we screened random-peptide phage display libraries for binding to G $\beta_1\gamma_2$ and identified a series of peptides that bound to a single preferred protein-protein interaction surface ("hotspot") on G β (3). One of the peptides (SIRK) blocked G $\beta\gamma$ -dependent regulation of PLC β_2 and PI3K γ but not regulation of type I adenylyl cyclase or N-type Ca $^{2+}$ channels, thus demonstrating the potential for selective targeting of G $\beta\gamma$ signaling. The crystal structure of G $\beta_1\gamma_2$ in a complex with a SIRK peptide derivative (SIGK) reveals the preferred interaction surface as a region overlapping the G α -switch II domain binding surface on top of the G β propeller (4–6). Subclasses of peptides appeared to bind distinct subsurfaces of the hotspot and differentially affect G protein subunit interactions. Many G $\beta\gamma$ effectors also use diverse mechanisms for binding within this surface (7, 8), and because peptides showed some selectivity, we hypothesized that small organic molecules also might selectively modulate G $\beta\gamma$ -target interactions.

We used FlexX virtual screening software (9) in the Sybyl molecular modeling package to dock 1990 compounds in the chemical diversity set from the National Cancer Institute (NCI) to the interaction hotspot of G $\beta_1\gamma_2$. The diversity library was designed to contain chemical core structures representative of the larger 250,251-compound library from NCI. The docked models were ranked using five scoring functions in C-Score: D-score, G-score, F-score, Chemscore, and PMF-score (10). Two consensus scores that equally weight the five scoring functions were also used to rank the compounds. The top 1% of compounds from each scoring function (85 compounds total) were tested for their ability to compete with phage-displaying SIGK for binding to biotinylated G $\beta_1\gamma_2$ (bG $\beta_1\gamma_2$) in an enzyme-linked immunosorbent assay (ELISA) (3). Nine of the 85 compounds inhibited SIGK binding with median inhibitory concentration (IC $_{50}$) values ranging from 100 nM to 60 μ M (Fig. 1B and table S1).

One compound, M119, with a high apparent affinity for bG $\beta_1\gamma_2$ (ELISA IC $_{50}$ = 200 nM) (Fig. 1, B and C, and table S1) was selected as a lead to define structure-activity requirements (SAR) for binding to G $\beta_1\gamma_2$.

Twenty-one compounds from the NCI library with similar structures to M119 were tested for relative G $\beta_1\gamma_2$ binding affinities (Fig. 1C and table S2). For example, the apparent affinity of M119B for bG $\beta_1\gamma_2$ is $1/1000$ that of M119, with the key chemical difference being the loss of two hydroxyl groups. Thus, specific chemical characteristics may be required for interactions with the G $\beta\gamma$ hotspot. We next tested whether M119 could disrupt protein interactions with a bona fide G $\beta\gamma$ binding partner, G α_{i1} . The hotspot for protein interaction overlaps with the G α switch II binding surface on G $\beta\gamma$. The overall G α_{i1} - $\beta\gamma$ interaction surface spans 1800 Å^2 (5, 6), and the dissociation constant (K $_d$) for G α_{i1} binding to G $\beta\gamma$ is ~ 1 nM (11). M119 competed with fluorescein isothiocyanate (FITC)- α_{i1} (F α_i) for binding to bG $\beta_1\gamma_2$ with an IC $_{50}$ value of 400 nM (Fig. 1D). However, unlike SIGK and related peptides that bind to this surface (12), M119 did not promote dissociation of G α_i from G $\beta\gamma$ (fig. S1).

FlexX docking software predicted that compounds M201 and M119 (Fig. 1C) bound to distinct subsurfaces in the hotspot, but M201 did not compete for SIGK binding. Nevertheless, we tested M119 and M201 in *in vitro* reconstitution assays of G $\beta\gamma$ -dependent activation of PLC β_2 , PLC β_3 , and PI3K γ and binding to GRK2. M119 attenuated G $\beta_1\gamma_2$ -dependent activation of PLC β_2 (IC $_{50}$ value of 3 μ M), PLC β_3 , and PI3K γ (Fig. 2, A to C, left panels). M201, on the other hand, did not affect PLC β_2 activation by G $\beta_1\gamma_2$ but potentiated G $\beta_1\gamma_2$ -dependent activation of both PLC β_3 and PI3K γ (Fig. 2, A to C, right panels). M119 also inhibited direct binding of bG $\beta_1\gamma_2$ to PLC β_2 and PLC β_3 , whereas M201 did not block binding of PLC β_2 and enhanced binding of PLC β_3 to G $\beta_1\gamma_2$ (fig. S2). M119 and M201 both inhibited GRK2 binding to bG $\beta_1\gamma_2$ with similar IC $_{50}$ values of approximately 5 μ M (Fig. 2D). A weakly binding compound M119B (Fig. 1C and table S2) did not have effects in these assays (fig. S3). These

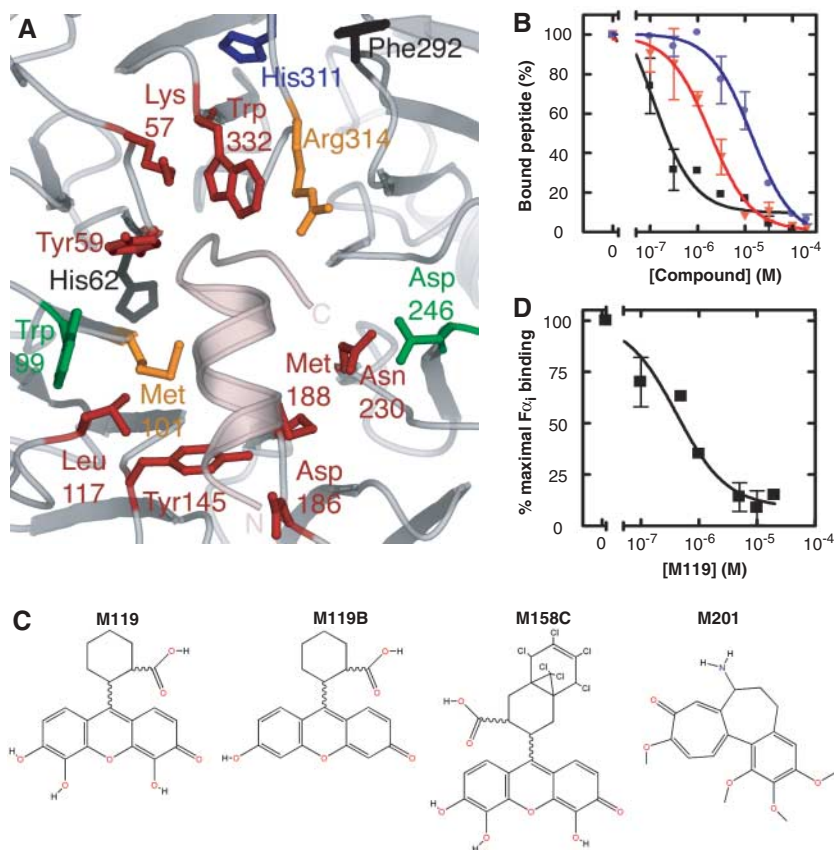


Fig. 1. Small molecule binding to the hotspot on G $\beta\gamma$. **(A)** Structure of SIGK bound to G $\beta\gamma$ at the hotspot. Amino acids within 6.5 Å of SIGK were targeted with the FlexX module of Sybyl virtual docking software. **(B)** Competition ELISA data for three of the compounds identified in the virtual screen. Compounds were tested for their ability to inhibit binding of a phage displaying the peptide SIGKAFKILGYPDYD (3, 4). M119 (NSC119910) (squares); M109 (NSC109208) (triangles); M117 (NSC117079) (circles). Data for all the binding compounds are summarized in table S1. **(C)** Structures of representative $\beta\gamma$ -binding compounds. **(D)** Competition of M119 for interactions between G α_{i1} and G $\beta_1\gamma_2$. F- α_{i1} and M119 were simultaneously added to bG $\beta_1\gamma_2$ immobilized on streptavidin beads. The amount of bead-based fluorescence was assessed by flow cytometry as described (11, 12).

¹Department of Pharmacology and Physiology and ²Department of Biochemistry and Biophysics, University of Rochester School of Medicine and Dentistry, Rochester, NY 14642, USA. ³Department of Genetics and Developmental Biology, University of Connecticut Health Center, Farmington, CT 06030, USA.

*To whom correspondence should be addressed. E-mail: Alan_Smrcka@URMC.rochester.edu

data suggest that both M201 and M119 bind to G $\beta\gamma$ but differentially modulate G $\beta\gamma$ interactions with effectors. These are only two of multiple diverse compounds identified, which suggests the potential for multiple modes of G $\beta\gamma$ -dependent target modulation by these small molecules.

To test the effects of differentially targeting G $\beta\gamma$ on GPCR signaling in intact cells, M119 (and a similar compound, M158C) (Fig. 1C and table S2) and M201 were tested for their ability to modulate fMLP receptor-dependent signaling in differentiated HL-60 leukocytes. The fMLP receptor couples to Gi in these cells and activates PLC β 2 (PLC β 3 is a minor isoform in these cells), PI3K γ , and ERK through G $\beta\gamma$ signaling (13, 14). Pretreatment of differentiated HL-60 cells with M119 and M158C (Fig. 3A and fig. S4A), but not M201 (Fig. 3B and

fig. S4B), attenuated fMLP-induced Ca $^{2+}$ increases. M119 had no effect on carbachol-dependent increases in Ca $^{2+}$ in HEK293 cells stably expressing the Gq-linked M3-muscarinic receptor, confirming a specific effect of M119 on G $\beta\gamma$ -dependent Ca $^{2+}$ mobilization (fig. S4C). fMLP-dependent GRK2 translocation to the membrane fraction of HL-60 cells, on the other hand, was substantially inhibited by incubation with either M119 or M201 (Fig. 3C). Thus, M119 and M201 differentially modulate PLC β 2 regulation by G $\beta\gamma$, yet both inhibit GRK2 binding in intact cells.

To assess the ability of M119 and M158C to inhibit fMLP receptor-dependent regulation of PI3K γ activation, we stimulated HL-60 cells stably overexpressing a green fluorescent protein (GFP)-tagged pleckstrin homology (PH) domain from Akt (15) with fMLP and assessed

translocation of the GFP-PHakt to the membrane by subcellular fractionation and Western blotting. The PH domain from Akt binds to PIP $_3$ produced by PI3K activity at the membrane. Pretreatment of the cells with 10 μ M of M119 or M158C inhibited fMLP-dependent translocation of GFP-PHakt to the membrane (Fig. 3D), consistent with the ability of these compounds to inhibit activation of PI3K γ by G $\beta\gamma$.

Stimulation of differentiated HL-60 cells with fMLP also results in pertussis toxin-sensitive activation of various MAP kinases, including ERK1 and ERK2, p38, and JNK (16). However, pretreatment of HL-60 cells with M119, M158C, and M201 did not block fMLP-induced activation of ERK1 and ERK2 (Fig. 3E). Ca $^{2+}$ mobilization occurred at low fMLP (100 nM) concentrations relative to that required to observe ERK1 and ERK2 (1 μ M) activation, indicating that the selective lack of effect of M119 on ERK activation is not due to excess G protein activation.

We tested the efficacy of our compounds in an *in vivo* model. Compared with wild-type animals, PLC β 3 $^{-/-}$ mice are 10 times as sensitive to the antinociceptive effects of the μ -agonist morphine (17). Because M119 blocks G $\beta\gamma$ -dependent activation of PLC β 3, we tested whether coadministration of M119 with morphine would also increase morphine-induced antinociception. Coadministration of M119 with morphine intracerebroventricularly resulted in an 11-fold increase in the analgesic potency of morphine (Fig. 4A) [ED $_{50}$ values and 95% confidence limits: 0.069 (0.023 to 0.201) nmol and 0.743 (0.341 to 1.62) nmol, respectively], whereas administration of 100 nmol M119 alone had no effect on baseline antinociception (table S3). M119 also had no effect on morphine-dependent antinociception in PLC β 3 $^{-/-}$ mice (Fig. 4B). These data highlight the specificity of M119 actions and the selective nature of M119 both *in vitro* and *in vivo*. G $\beta\gamma$ subunits regulate many aspects of signaling critical for the actions of opioid agonists (18). If M119 were globally blocking G $\beta\gamma$ subunit functions, we expect that morphine-induced antinociception would have been attenuated rather than potentiated with M119 coadministration.

Protein interaction interfaces present difficult drug targets because of the generally large interaction surface area and flat topology of the interaction surfaces. Hotspots at protein interfaces comprise a small fraction of the overall interaction surface, yet are responsible for most of the energetics of binding, and it has been proposed that targeting such surfaces could successfully disrupt protein-protein binding (19). As a result of extensive screening, some protein interaction interfaces have been targeted with small molecules (19–21). Our screen of only 1990 molecules identified multiple compounds with apparent affinities in the high nM

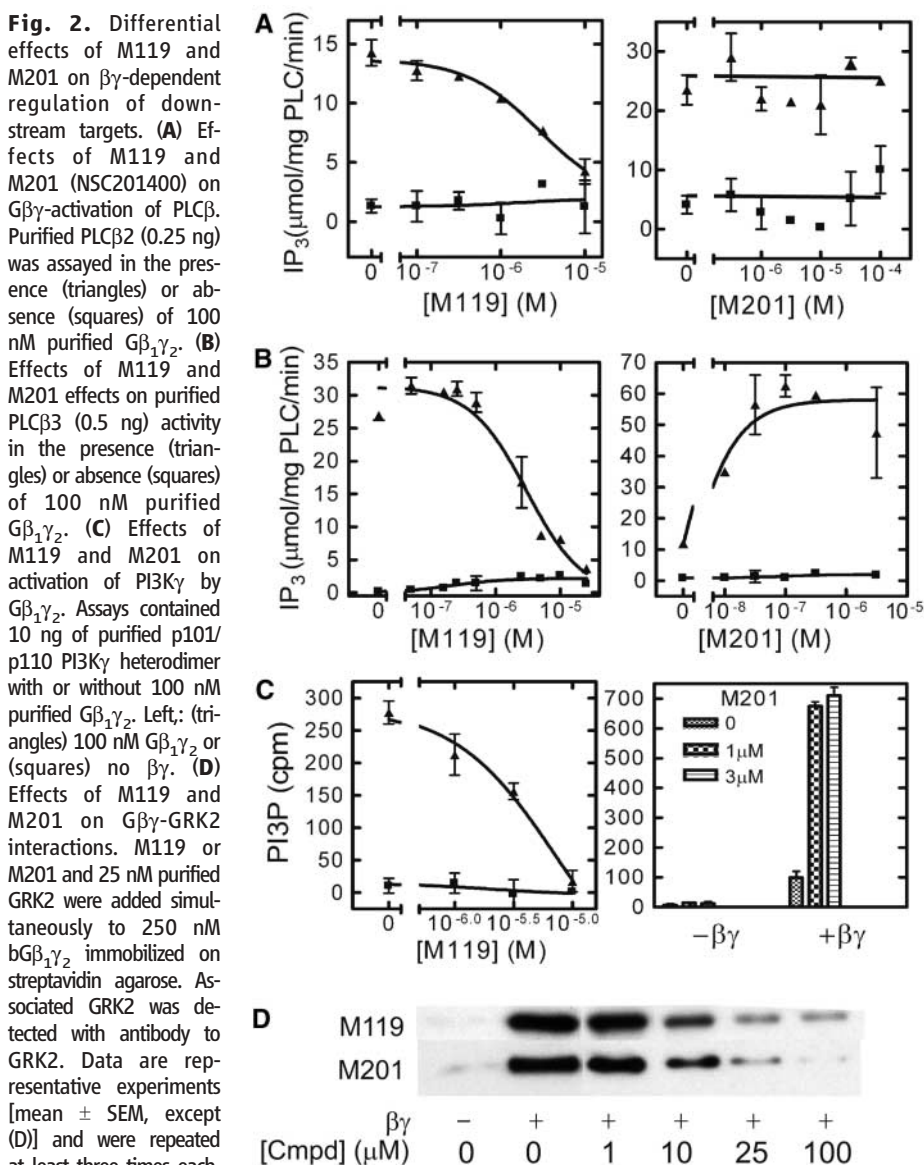


Fig. 3. Effects of M119 and related compounds on G $\beta\gamma$ signaling in dimethyl sulfoxide (DMSO)-differentiated HL-60 cells. **(A)** M119 and related compounds block fMLP-dependent Ca²⁺ release in differentiated HL-60 cells, loaded with 1 μ M Fura2-AM. Cells were pretreated with DMSO or 10 μ M compounds for 5 min before stimulation with 250 nM fMLP. The change in fluorescence was monitored at 340/380 nm. Data are representative of five independent experiments. Compounds are significantly different than DMSO control, $P < 0.01$. See fig. S4A for dose dependence. **(B)** Same as A except 10 μ M M201 was tested. Data are representative of four independent experiments. See fig. S4B for pooled data. **(C)** M119 and M201 inhibition of GRK2 translocation. Differentiated HL-60 cells were treated with 10 μ M compound before stimulation with 250 nM fMLP. Translocation of endogenous GRK2 was determined by Western blotting with a GRK2 antibody and quantitative chemiluminescence. Data are mean \pm SEM from five experiments, * $P < 0.05$, ** $P < 0.01$ analysis of variance (ANOVA). **(D)** M119 and M158C (NSC158110) inhibition of GFP-PHAkt translocation. Differentiated HL-60 cells stably overexpressing GFP-PHAkt were treated with 10 μ M compound before stimulation with 100 nM fMLP. Translocation of GFP-PHAkt to the membrane was determined by Western blotting with antibody to GFP and quantitative chemiluminescence. Data are mean \pm SEM from four experiments. *** $P < 0.001$ ANOVA. **(E)** Lack of effect of M119, M158C, and M201 on fMLP-induced ERK1 and ERK2 activation. Differentiated HL-60 cells were pretreated with 10 μ M of compound prior to stimulation with 1 μ M fMLP for 5 min. Levels of phosphorylated and total ERK were determined by Western blotting. This experiment was repeated three times with similar results.

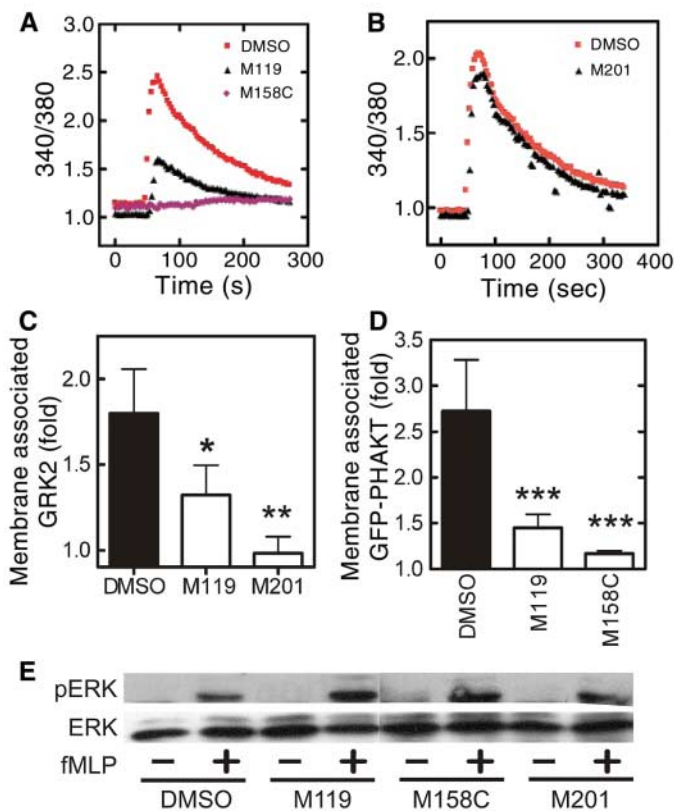
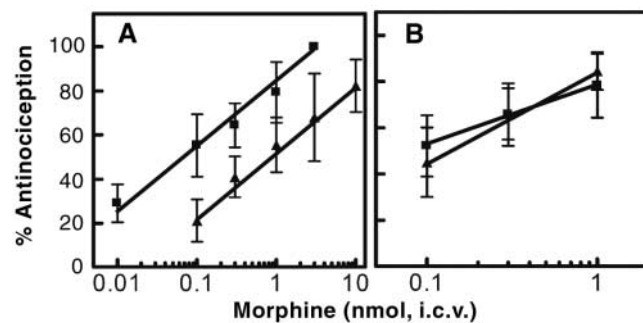


Fig. 4. M119 effects on morphine-induced antinociception in **(A)** wild-type and **(B)** PLC $\beta 3^{-/-}$ mice. Increasing concentrations of morphine were administered intracerebroventricularly to mice with (squares) or without (triangles) concomitant administration of 100 nmol M119. Antinociception was measured 20 min after injection using the 55°C tail-flick test. Data are mean \pm SEM from 7 to 10 animals at each point.



to low μ M range. These molecules demonstrate that multiple small molecule binders of G $\beta\gamma$ could be developed that differentially modulate functions downstream of GPCRs. Numerous studies in animal models have implicated G $\beta\gamma$ -subunit targeting as a therapeutic strategy in diseases such as heart failure (22), prostate cancer (23), vascular disease (24), and inflammatory disease (13). Thus, more extensive screening for molecules that bind to the G $\beta\gamma$ hotspot will yield a repertoire of potentially therapeutically useful small molecules.

References and Notes

- D. E. Clapham, E. J. Neer, *Annu. Rev. Pharmacol. Toxicol.* **37**, 167 (1997).
- T. M. Cabrera-Vera et al., *Endocr. Rev.* **24**, 765 (2003).
- J. K. Scott et al., *EMBO J.* **20**, 767 (2001).
- T. Davis, T. M. Bonacci, A. V. Smrcka, S. R. Sprang, *Biochem.* **44**, 10593 (2005).
- M. A. Wall et al., *Cell* **83**, 1047 (1995).
- D. G. Lambright et al., *Nature* **379**, 311 (1996).
- C. E. Ford et al., *Science* **280**, 1271 (1998).
- Y. Li et al., *J. Biol. Chem.* **273**, 16265 (1998).
- M. Rarey, B. Kramer, T. Lengauer, G. Klebe, *J. Mol. Biol.* **261**, 470 (1996).
- R. D. Clark, A. Strizhev, J. M. Leonard, J. F. Blake, J. B. Matthew, *J. Mol. Graph. Model.* **20**, 281 (2002).
- N. A. Sarvazyan, A. E. Remmers, R. R. Neubig, *J. Biol. Chem.* **273**, 7934 (1998).
- M. Ghosh, Y. K. Peterson, S. M. Lanier, A. V. Smrcka, *J. Biol. Chem.* **273**, 34747 (2003).
- Z. Li et al., *Science* **287**, 1046 (2000).
- E. R. Neptune, H. R. Bourne, *Proc. Natl. Acad. Sci. U.S.A.* **94**, 14489 (1997).
- G. Servant et al., *Science* **287**, 1037 (2000).
- M. J. Rane, S. L. Carrithers, J. M. Arthur, J. B. Klein, K. R. McLeish, *J. Immunol.* **159**, 5070 (1997).
- W. Xie et al., *Proc. Natl. Acad. Sci. U.S.A.* **96**, 10385 (1999).
- M. Connor, M. J. Christie, *Clin. Exp. Pharmacol. Physiol.* **26**, 493 (1999).
- M. R. Arkin, J. A. Wells, *Nat. Rev. Drug Discov.* **3**, 301 (2004).
- A. G. Cochran, *Curr. Opin. Chem. Biol.* **5**, 654 (2001).
- T. Oltersdorf et al., *Nature* **435**, 677 (2005).
- G. Iaccarino, W. J. Koch, *Assay Drug Dev. Technol.* **1**, 347 (2003).
- Y. Daaka, *Sci. STKE* **2004**, re2 (2004).
- G. Iaccarino, L. A. Smithwick, R. J. Lefkowitz, W. J. Koch, *Proc. Natl. Acad. Sci. U.S.A.* **96**, 3945 (1999).
- We thank the Developmental Therapeutics Program at the NCI/NIH for providing the compounds used in this study, J. Benovic for providing purified GRK2, H. Bourne for providing HL-60 cells stably overexpressing GFP-PHAkt, and S. Sprang for evaluation of this manuscript. Supported by NIH grants GM60286 (A.V.S.), K05-DA00360 (J.M.B.), HL080706 (D.W.), Predoctoral Training grant in Cardiovascular Biology HL-T3207949 (T.M.B.), and NIDA Drug Abuse Training grant T32DA07232 (J.L.M.).

Supporting Online Material

www.sciencemag.org/cgi/content/full/312/5772/443/DC1
Materials and Methods
Tables S1 to S3
Figs. S1 to S4
References

20 September 2005; accepted 28 February 2006
10.1126/science.1120378